HST/WFPC2 analysis of the mid-UV and optical colors within the disks of nearby galaxies

S. C. Odewahn[1], **R. A. Jansen**[1], **R. A. Windhorst**[1], **V. Taylor**[1], **P. Eskridge**[2]

[1]***Dept. of Physics and Astronomy, Arizona State University,***
[2]***Dept. of Physics and Astronomy, Minnesota State University***

ABSTRACT

We have used WFPC2 in Cycle 9 (GO) and Cycle 10 (SNAP) programs to image 64 nearby galaxies in F300W and F814W for the primary purpose of studying the morphological properties of galaxies in the near-UV. Sample selection, described in Windhorst etal 2002 (ApJS,143,Nov), was designed to include galaxies of all types, including dwarf systems, but was preferentially skewed towards the late Hubble types. Our ultimate goal is to use these data as a benchmark for comparing the morphological properties of nearby and high redshift systems, where the latter are observed predominantly in a restframe bandpass in the mid-UV. In this poster we present classical radial surface brightness profiles, and review our analysis of 64 galaxies following the Fourier-based methodology of Odewahn etal 2002 (ApJ,568,539) and the pixel color map approach of Eskridge etal 2002 (ApJ submitted). Our near-ultraviolet and optical images reveal regions of strong on-going star formation that are sometimes associated with structures traced by the old stellar populations. We will use our F300W-F814W pixel color-magnitude diagrams to quantify the level and character of star formation in the outer regions (beyond the effective radius) of our disk-dominated galaxies.

We acknowledge support from NASA grants AR.6385.01.95A, GO-8645.01-00, GO-9124.01-02, and AR-7534.01-96A.

1. INTRODUCTION

The UV properties of galaxies are poorly understood compared to SED regimes redward of the 4000 angstrom break. Unfortunately, it is this part of the rest-frame SED we are using to observe distant galaxies with filters as red as F814W and $z \gtrsim 1$.

This situation will not improve drastically with ACS. How are the morphological properties we infer from a galaxy image dependent on rest-frame bandpass? We have conducted WFPC2 programs in Cycles 9 and 10 primarily to address this issue, but a host other interesting questions are being addressed with these images.

2. THE SAMPLE

Our observing methods and sample selection criteria are described in Windhorst et al. 2002. For the purpose of this conference, we have broken our current sample of 64 galaxies observed in F814W and F300W into 3 groups: dwarf galaxies (Table 1), giant galaxies (Table 2), and morphologically peculiar and/or merging/interacting systems (Table 3). We have cross-matched our sample with the RC3 to obtain radial velocity, V_{GSR}, and total magnitude, B_T, in order to compute an *approximate* absolute magnitude, M_B, assuming $H_0 = 65 km/s/Mpc$. WFPC2 image registration and stacking were performed with LMORHO (Odewahn et al. 1997; AJ,114,2219). To make a qualitative comparison among these galaxies, we used surface brightness images (calibrated following Holtzmann et al. 1995) to construct color images for all of our galaxies. In Figures 1 through 3 we show examples of dwarf systems (Table 1), giant systems (Table 2), and merging or peculiar systems (Table 3).

3. SURFACE BRIGHTNESS PROFILE ANALYSIS

We have used the LMORPHO software system to measure radial surface brightness profiles in *matched* elliptical apertures for each galaxy (i. e. each elliptical annulus in the F814W and F300W images is spatially the same). Examples of the SB profiles extracted in this manner are shown in Figures 4 through 12 along with SB-calibrated grey-scale galaxy images from each bandpass. The light-ellipse in each image shows the position of the outer-most profile annulus, and the bold-ellipse shows the effective radius, r_e in each band. These data are being used to perform luminosity decompositions and to determine the radial color profile trends in the outer regions of our galaxies. Using radial profiles, with the radial scale normalized by r_e, we are computing mean SB and color profiles in various galaxy groupings to uncover any global trends in the outer areas of galaxies that may be useful for interpreting high redshift galaxy morphology.

4. FOURIER-BASED and COLOR-PIXEL ANALYSES

In Odewahn et al. 2002 we have developed a Fourier-based method of characterizing and classifying *morphological* structure in galaxy images. We have adapted a moments-based image analysis technique (Odewahn 1989) to fit Fourier components to fixed-grid azimuthal profiles in elliptical annuli to reconstruct galaxy images. One may think of this step as an optimized data compression technique for reducing the dimensionality of our ultimate pattern classification problem: the recognition and characterization of morphological features in galaxies. An example illustrating this method is shown in Figure 13. In Figure 14 we show a type-dependent parameter space produced with this approach. In the context of this work, we are in the process of using the zeroeth Fourier moment profiles to construct radial SB profile (as in the previous section) that are free of the influence of high spatial frequency image structure.

We show an example of the color pixel analysis of NGC 6753 in Figures 15 and 16 from Eskridge et al. 2003. This approach is similar to that of Bothun (1986), who first made a pixel color-magnitude diagram (pCMD) for NGC 4449. These plots indicate that the blue plumes are due to plateaus in the I_{814}-band surface brightness of the disks, with no difference in their average NUV surface brightnesses. Thus the separation of the blue plumes is due to drops in the I_{814}-band surface brightness at particular radii. Further, as the NUV surface brightness distribution is the same in the two plumes, this means the drops in the I_{814}-band surface brightness have essentially no effect on the absolute strength of the on-going star formation. We speculate that the abrupt changes in the I_{814}-band surface brightness are due to dynamical effects in the disks of the galaxies that govern the long-term global star formation in the disks.

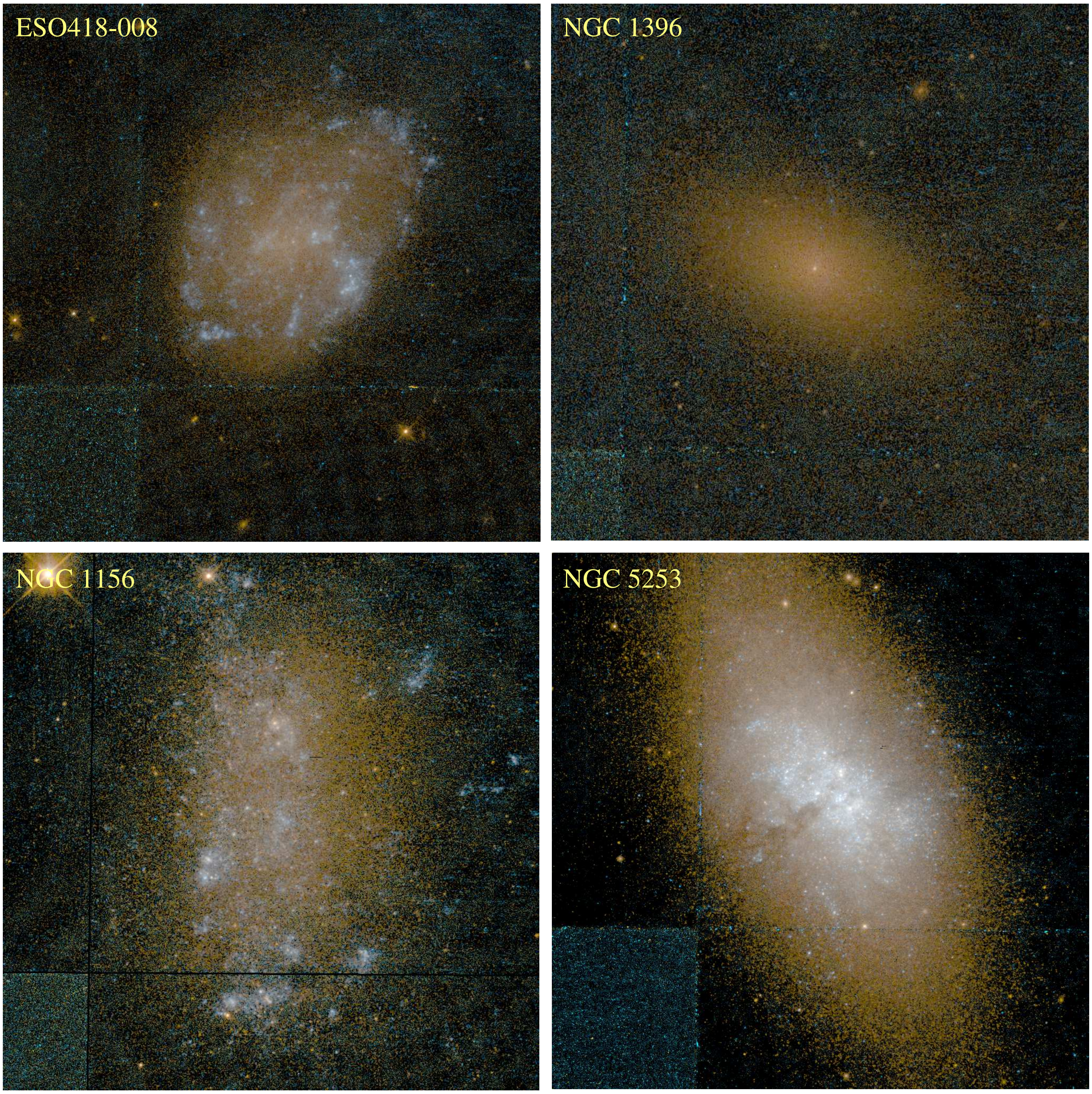

Fig. 1.— Dwarf systems in our survey.

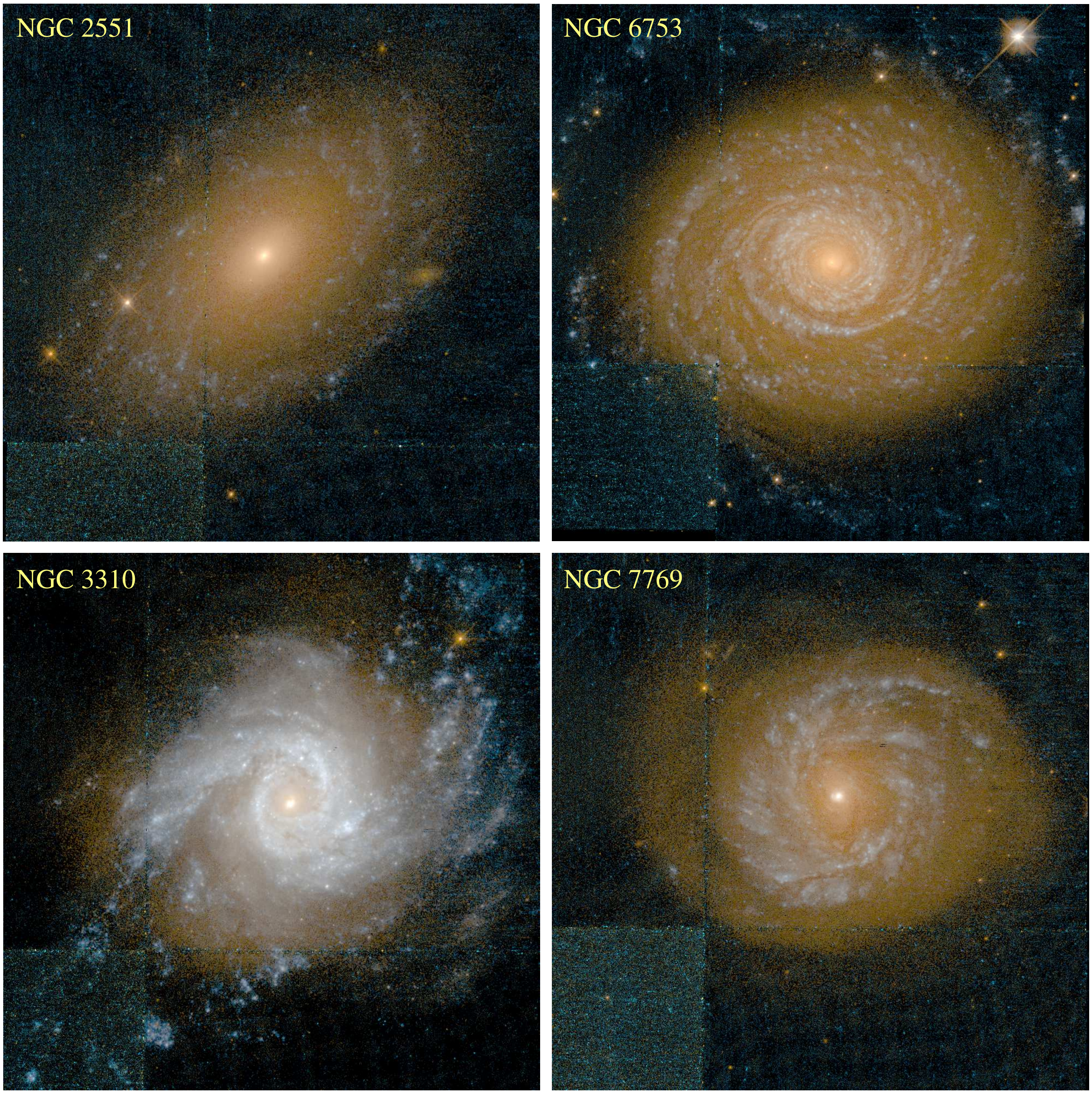

Fig. 2.— Giant systems in our survey. Note that NGC 7769 = UGC 12808.

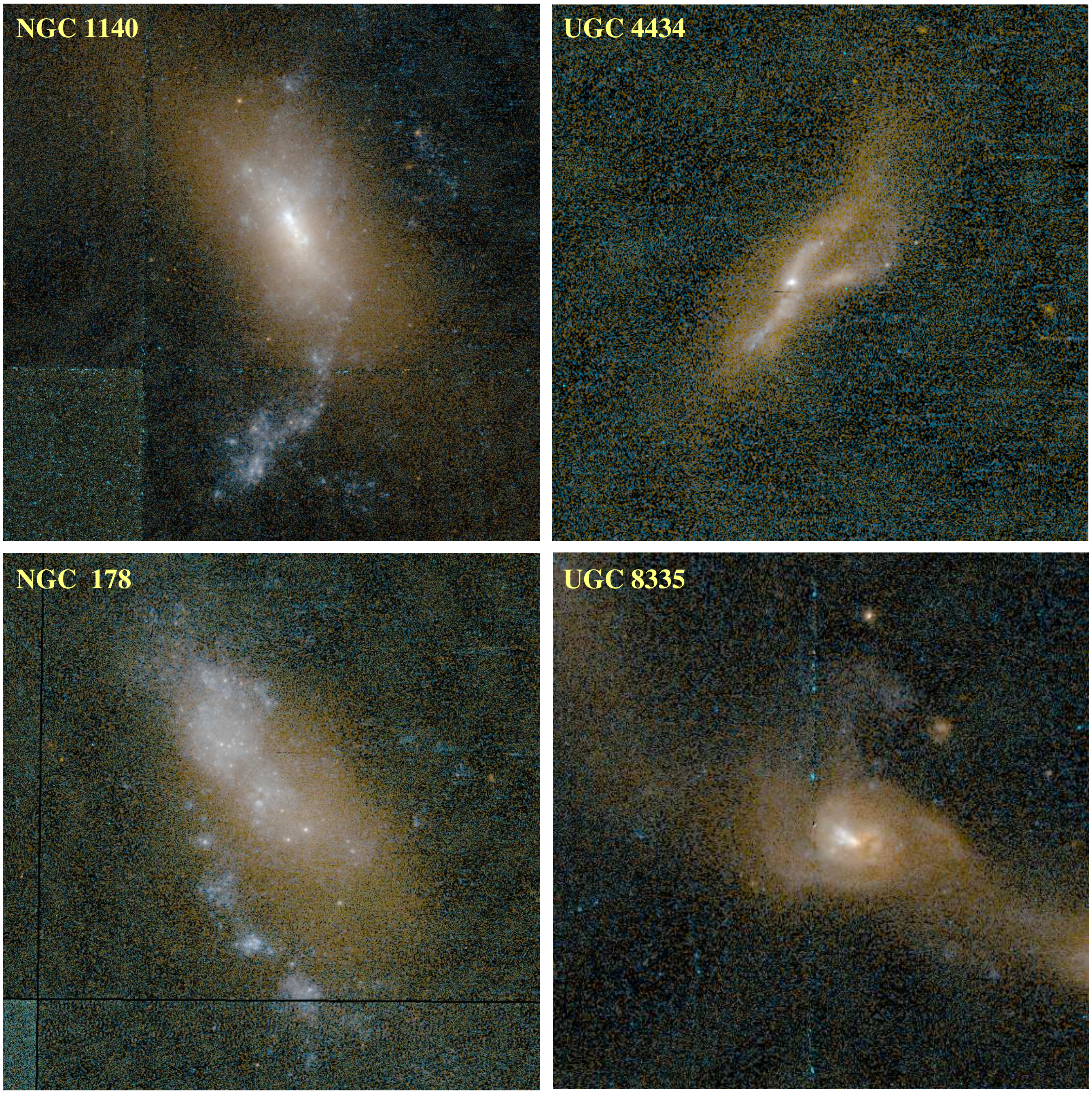

Fig. 3.— Merging and/or peculiar systems in our survey.

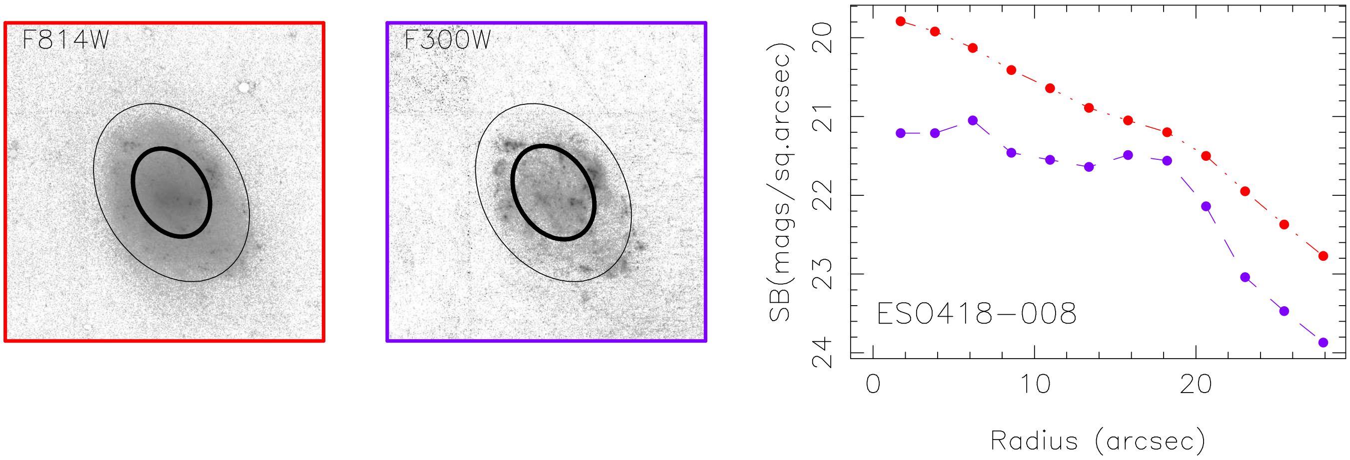

Fig. 4.— ESO418-008, a dwarf system in our survey.

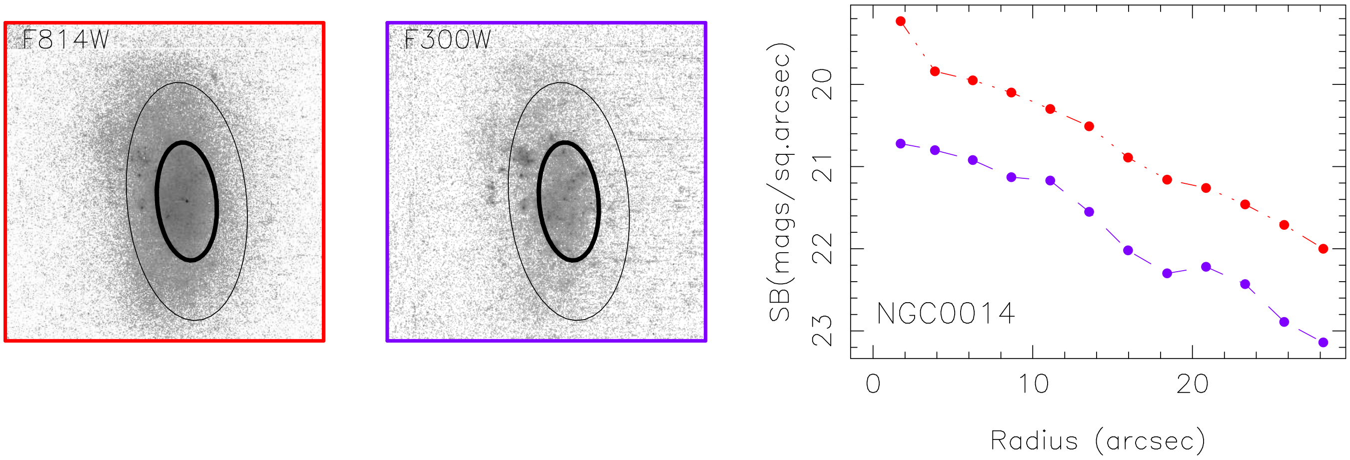

Fig. 5.— NGC 14, a dwarf system in our survey.

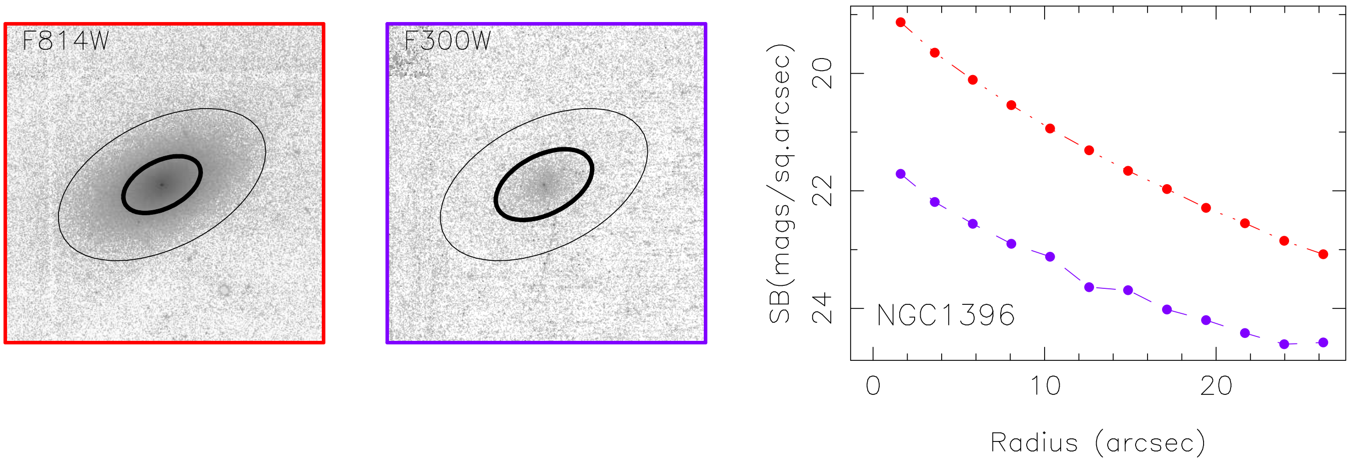

Fig. 6.— NGC 1396, a (nucleated) dwarf system in our survey.

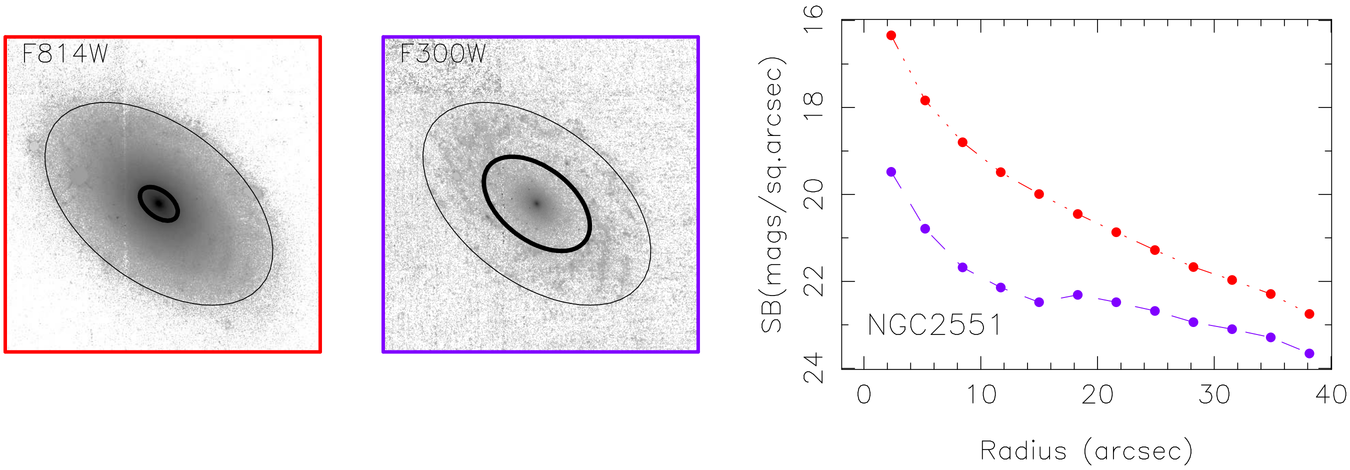

Fig. 7.— NGC 2551, a giant galaxy in our survey.

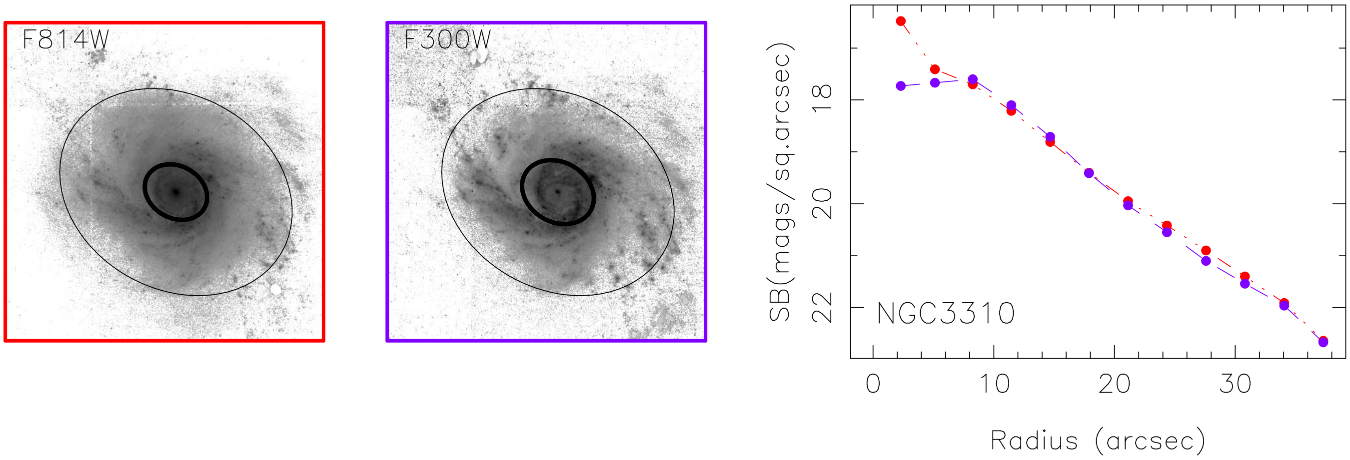

Fig. 8.— NGC 3310, a high surface brightness giant galaxy in our survey.

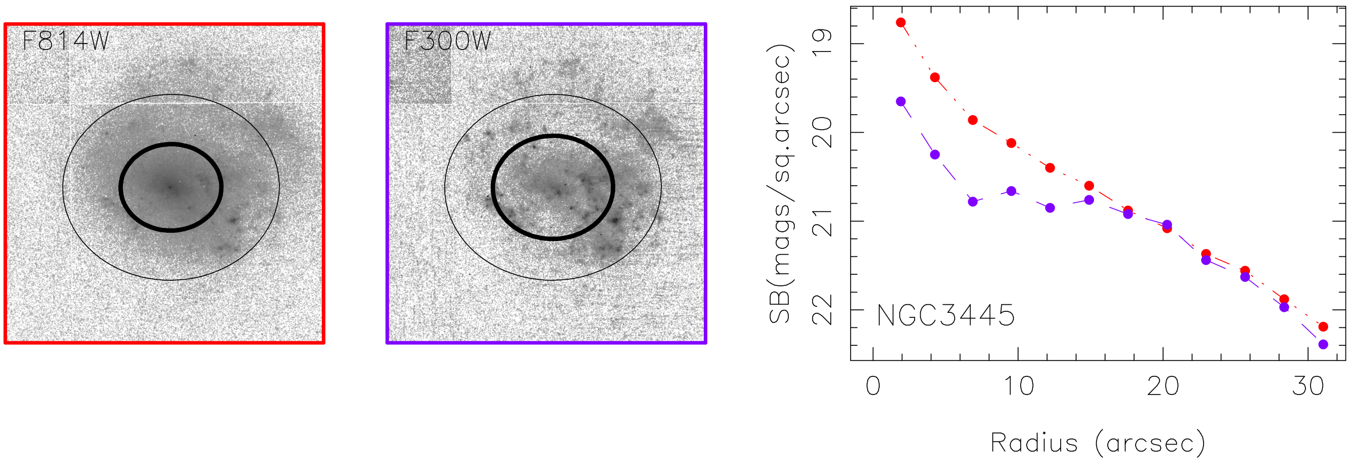

Fig. 9.— NGC 3445, a giant galaxy in our survey.

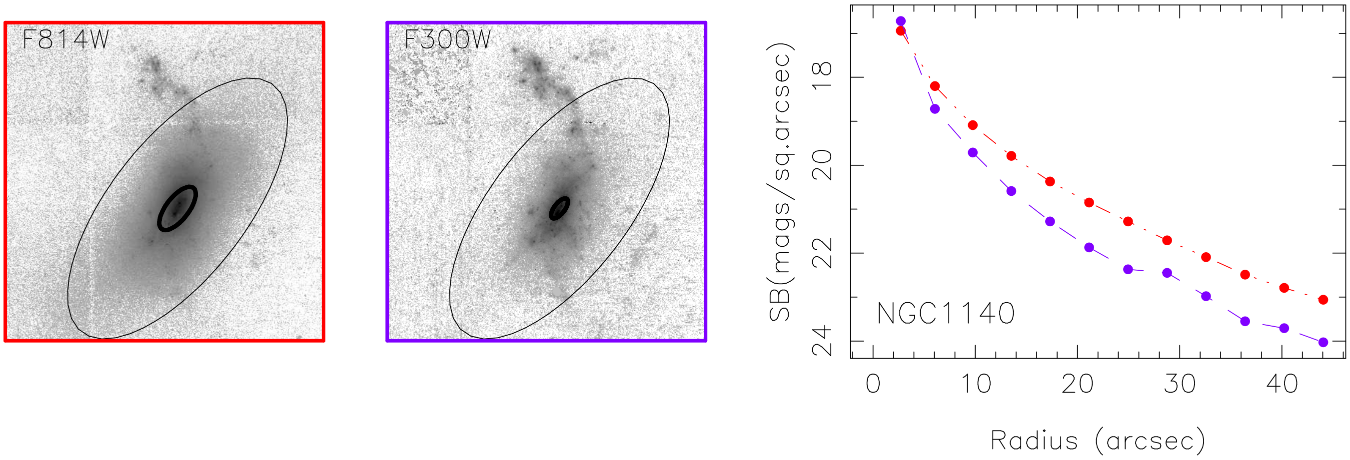

Fig. 10.— NGC 1140, a merging and/or peculiar system.

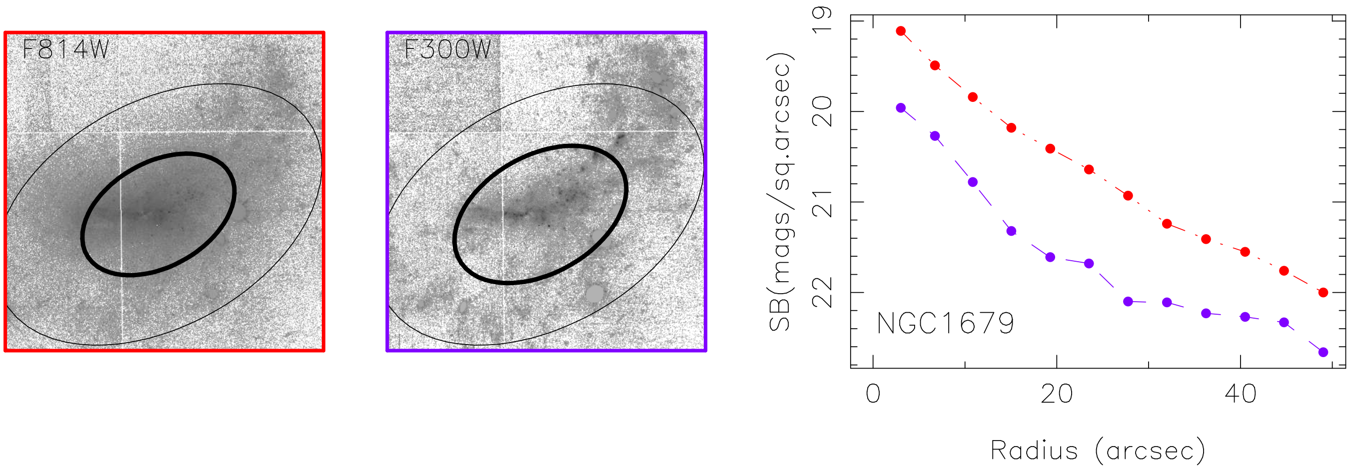

Fig. 11.— NGC 1679, a merging and/or peculiar system.

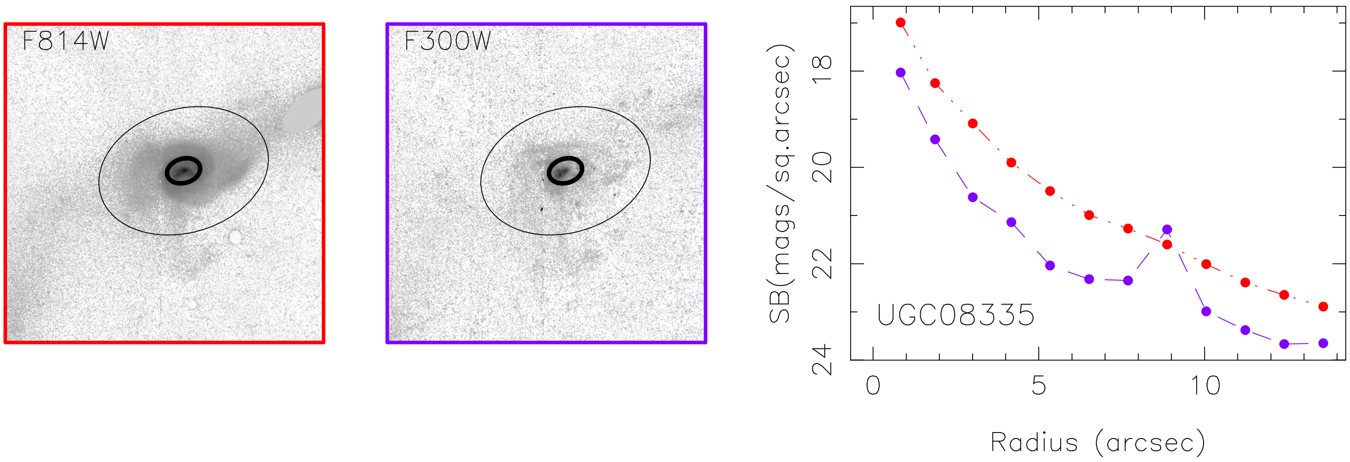

Fig. 12.— NGC 8335, a merging and/or peculiar system.

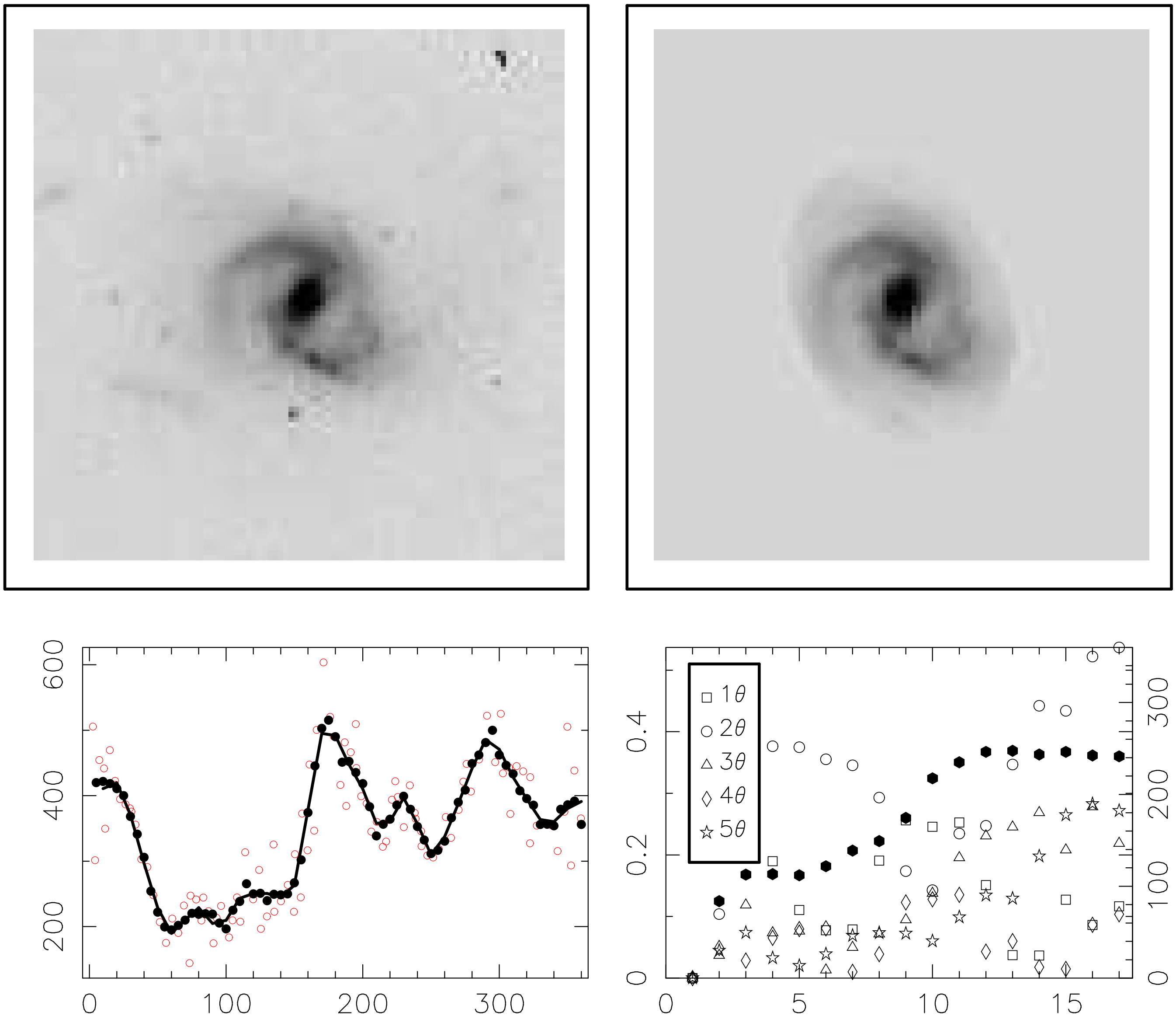

Fig. 13.— The Fourier image-modeling method described in Odewahn et al. (ApJ,568,539) applied to a galaxy observed with HST in the B-Band Parallel Survey (BBPS, Cohen et al. 2001, AJ-submitted). The original F814W image is shown in the upper-left panel, and the Fourier model image is shown in the upper-right. In the lower-left panel we plot the azimuthal profile for the annulus over-plotted in the galaxy image. Open circles are individual pixel values, solid points represent the smooth points, and the solid line represents the Fourier series fitted to this profile. In the lower-right panel we plot the five Fourier amplitudes as a function of radial annulus number using open symbols (left numeric scale). Finally, the solid points represent the phase angle, measured in degrees in the equatorial plane, of the 2θ component (right numeric scale).

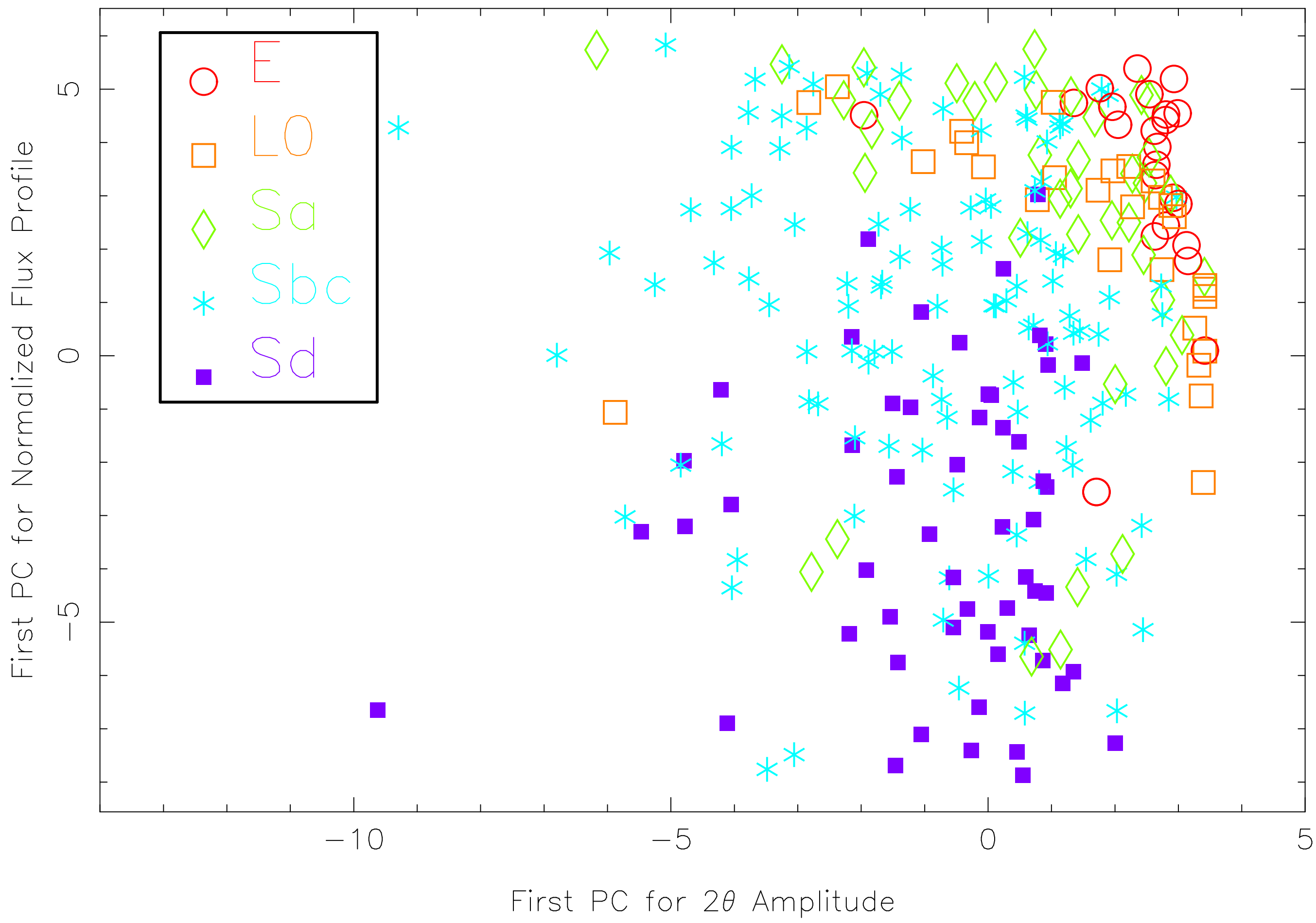

Fig. 14.— The first principal components formed from an analysis of the 2θ amplitude and normalized flux profiles from 246 local and distant galaxies. We see a clear segregation by revised Hubble stage (normally referred to as the Hubble type). A variety of independent and similarly fuzzy Fourier-based image parameter may be combined via artificial neural network (ANN) image classifiers to predict stage values. An important aspect of current work is to address how such parameter spaces change systematically as we observe blueward of the 4000 angstrom break or as we observe progressively fainter (in absolute magnitude) galaxies.

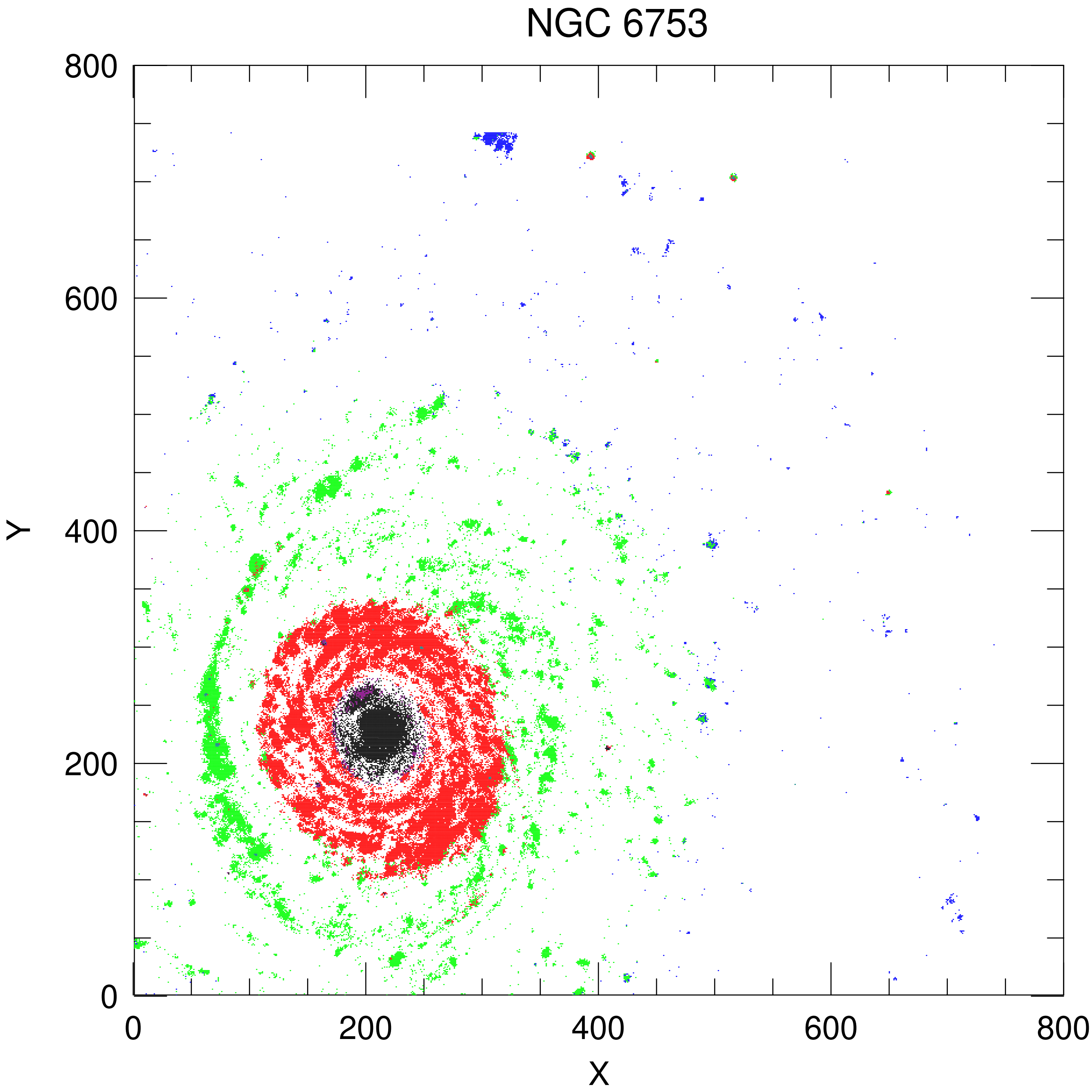

Fig. 15.— Spatial map of NGC 6753 showing the locations of the pixels in the red plume (black points), blue plume 1 (red points), blue plume 2 (green points), and the very blue smear (blue points).

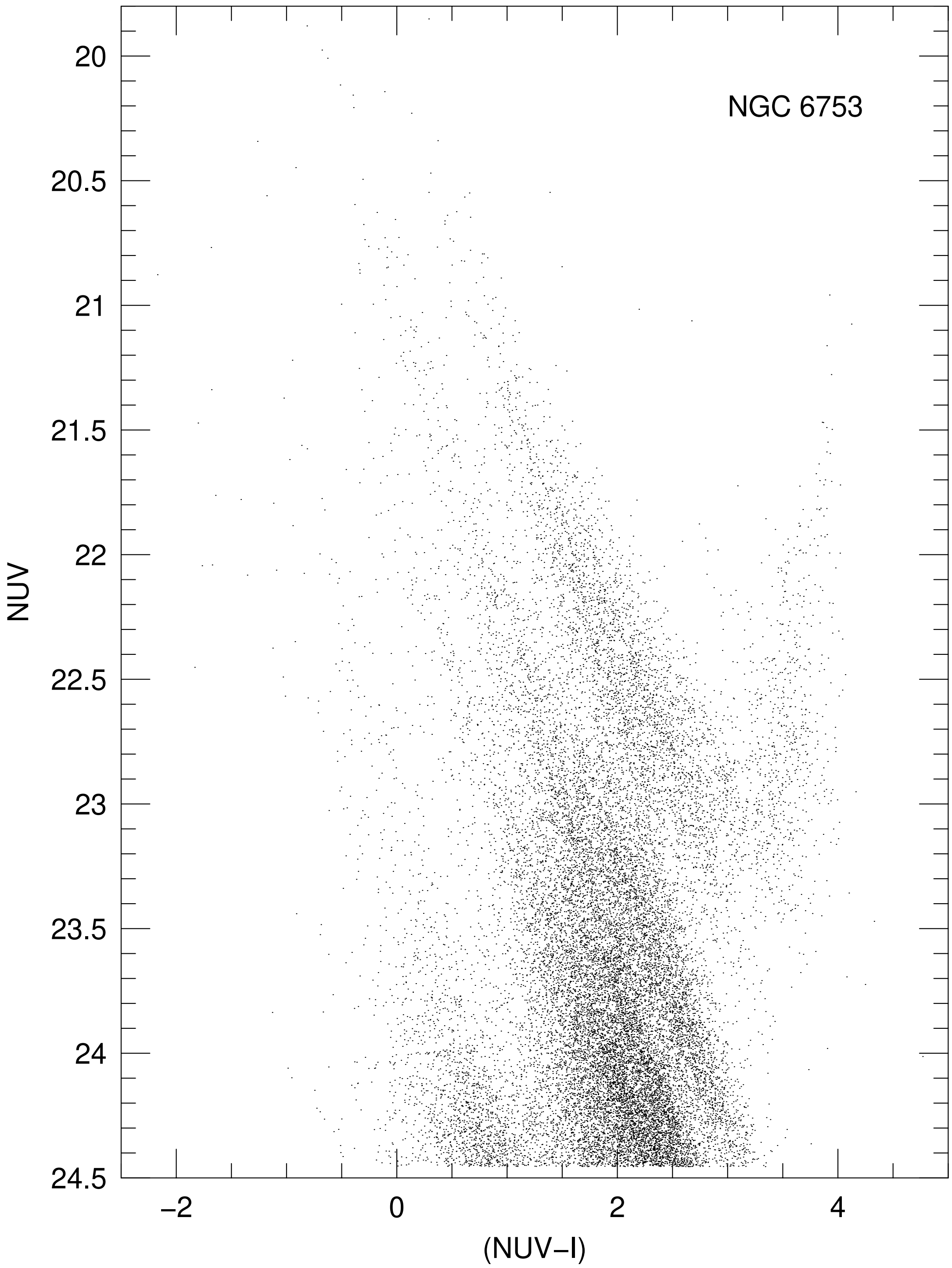

Fig. 16.— Binned NUV — $(NUV - I_{814})$ pCMDs for NGC 6753 with with 3×3 pixel binning. At lower surface brightness, some interesting features emerge. The red plume has a clear faint limit (at $NUV \approx 23.5$), much brighter than the S/N cut-off imposed. This limit is the minimum NUV surface brightness of the old population in the bulge region of NGC 6753.

Table 1. HST-WFPC2 Sample 1 - Nearby Dwarf Galaxies

$\alpha(J2000)\delta$	Name	M_B	V_{GSR}	RC3 Type	T_{rc3}	T_{F300W}	T_{F814W}
03:31:30.37 -30:12:42.4	ESO 418-8	-16.8	1146	.SXT8..	Sdm	Sd	Scd
05:31:50.53 -23:08:43.5	IC 2130	-17.9	1671	.SBS8..	Sdm	Im	
11:33:29.34 -26:56:47.9	ESO 503-22	-17.0	1726	.IBS9*P	Im	Im	
00:08:46.01 +15:48:53.9	NGC 14	-17.6	1012	RIBS9P.	Im	Im	Im
02:59:42.10 +25:14:14.1	NGC 1156	-17.0	452	.IBS9..	Im	Im	Im
03:20:06.62 -52:11:14.1	NGC 1311	-15.0	331	.SBS9?	Sm	Im	Im
03:38:06.65 -35:26:24.5	NGC 1396	-14.8	771	.LX.-*.	S0-	cE	cE
05:06:25.74 -31:57:12.8	NGC 1800	-16.3	637	.IBS9..	Im	Im	Im
13:39:56.39 -31:38:29.1	NGC 5253	-16.8	271	.I..9P*	Im	Im	Im
01:32:42.42 +18:19:00.0	UGC 1104	-15.6	775	.I..9..	Im	Im	Im
16:33:47.78 +28:59:06.0	UGC 10445	-17.4	1102	.S..6?.	Scd		

Approximate absolute magnitude, M_B, computed using RC3 radial velocity and $H_0 = 65$. The T_{F300W},T_{F814W} morphological types are visual estimates by Odewahn. As with Tables 2 and 3, only the stage portion of revised Hubble system class is tabulated here. Galaxies are classed as B(bulge-domimated) or D(disk-domimated) if insufficient signal makes a full RHS estimate imposiible. As discussed in Windhorst et al. 2002, no strong morphological K-correction is evident for the majority of these late type systems.

Table 2. HST-WFPC2 Sample 2 - Nearby Giant Galaxies

$\alpha(J2000)\delta$	Name	M_B	V_{GSR}	RC3 Type	T_{rc3}	T_{F300W}	T_{F814W}
12:30:16.99 +12:19:44.5	NGC 4478	-18.5	1329	.E.2...	E	cE	cE
15:48:41.28 +21:52:10.4	UGC 10043	-18.5	2254	.S..4..	Sbc		Sa
11:32:36.91 +52:56:52.4	HICK 56C	-19.0	8175	PS..0P*	S0a	cE	Sa
11:06:48.85 +72:34:09.5	NGC 3516	-20.2	2749	RLBS0*.	S0	B	Sa
08:24:50.02 +73:24:46.3	NGC 2551	-19.2	2384	.SAS0..	S0a	Sab	Sab
23:41:47.28 -03:40:03.6	A 2339-03A	-21.1	6954	.S.5$P/	Sc		Sb
13:41:43.64 +55:40:23.3	NGC 5279		7694	.SBS1P.	Sa	Sbc	Sb
19:11:23.44 -57:02:53.2	NGC 6753	-21.0	3073	RSAR3..	Sb	Sb	Sb
19:23:57.27 -59:55:15.4	NGC 6782	-20.8	3815	RSXR1..	S0a	Sb	Sb
10:38:45.71 +53:30:16.7	NGC 3310	-19.3	1043	.SXR4P.	Sbc	Sbc	Sb
23:51:03.60 +20:08:58.0	NGC 7769	-20.7	4380	RSAT3..	Sb	Sb	Sb
13:39:53.21 +00:50:22.3	NGC 5257	-21.2	6758	.SXS3P.	Sb	Sc	Sbc
07:55:06.42 +55:42:14.3	A 0751+55	-20.6	6195	.S...P.		Sb	Sbc
23:30:33.06 +03:54:00.8	NGC 7685	-20.5	5775	.SXS5*.	Sc	Scd	Sbc
00:48:35.32 -12:42:59.6	A 0046-12		6447	RLB.0P?	S0	Sc	Sc
09:28:02.61 +68:25:08.6	UGC 5029	-19.5	3977	.SXS5..	Sc	Sd	Sc
12:58:56.36 +27:50:00.5	IC 3949	-19.4	7460	.LA..P/	S0	Sd	Sc
11:44:47.76 +19:46:22.8	MCG 3-30-87		8243			Sdm	Scd
10:54:35.24 +56:59:26.8	NGC 3445	-18.9	2092	.SXS9..	Sm	Im	Scd
11:44:02.13 +19:47:05.1	MCG 3-30-71	-18.7	4886	.S?....		Scd	Sd
09:27:50.13 +68:24:42.2	A 0923+68	-19.2	3801	.SBS8P.	Sdm	Sm	Sm
13:25:53.62 +57:15:14.7	A 1323+57		6638			Im	Im
19:16:42.35 +63:58:14.7	NGC 6789		-999	.I..9..	Im	Im	Im
23:02:59.11 +16:36:15.0	NGC 7468	-18.1	2271	.E.3.*P	E	Im	Im
11:43:48.88 +19:58:06.3	UGC 6697	-20.6	6678	.I..9*.	Im	Im	Im

Approximate absolute magnitude, M_B, computed using RC3 radial velocity and $H_0 = 65$. The T_{F300W},T_{F814W} morphological types are visual estimates by Odewahn. Galaxies in this list are ordered by T_{F814W}, with the early types listed first. In general, a significant morphological K-correction is present only amoung the early morphological types. NOTE: We exclude 14 galaxies from this set that were not matched to an RC3 source.

Table 3. HST-WFPC2 Sample 3 - Merging/Interacting/Peculiar Galaxies

$\alpha(J2000)\delta$	Name	M_B	V_{GSR}	RC3 Type	T_{rc3}	T_{F300W}	T_{F814W}
04:49:55.14 -31:58:03.0	NGC 1679	-18.0	904	.SBS9..	Sm	Im	MERG
00:39:08.27 -14:10:25.7	NGC 178	-18.4	1496	.SBS9..	Sm	MERG	Im
02:54:32.99 -10:01:46.2	NGC 1140	-18.4	1479	.IB.9P*	Im	MERG	MERG
09:35:51.40 +61:21:12.8							MERG
13:44:42.18 +55:53:11.9	A 1342+56		11390	.P.....	11.92	MERG	MERG
11:28:31.89 +58:33:44.4						MERG	MERG
08:28:54.44 +34:39:03.0	UGC 4434	-20.3	6256	.S?....		MERG	MERG
11:32:40.38 +52:57:05.1						Sb	MERG
13:15:30.37 +62:07:47.4						Im	MERG
13:41:39.46 +55:40:12.7	NGC 5278		7656	.SAS3$P	Sb	PEC	Sa
04:03:32.64 -43:24:05.8	NGC 1510	-16.3	838	.LA.0P?	S0	Im	PEC
06:15:35.09 +71:02:14.8	A 0609+71B	-19.8	4124	.L...*.	S0	PEC	cE
11:51:06.72 +55:04:48.0	NGC 3921	-21.1	5930	PSAS0P.	S0a	PEC	PEC
13:53:03.31 +69:18:31.0	A 1351+69	-20.5	9323	.L.....	S0	STELL	Sb
13:15:35.44 +62:07:25.4	UGC 8335		9364	.S?....		PEC	MERG

Approximate absolute magnitude, M_B, computed using RC3 radial velocity and $H_0 = 65$. The T_{F300W},T_{F814W} morphological types are visual estimates by Odewahn. M_B is not known for galaxies in this list not matched to the RC3, and hence some dwarf systems may be present. In addition to being astrophysically interesting in their own right, we included such systems in our nearby galaxy survey because they seem to form an important population fraction in the high redshift Universe.